UV/visible-light photocatalytic degradation of organic dyes using ZnO nanomaterials

Nguyen Thi Phuong[1], Lai Van Duy[2], Tran Van Chinh[1, 3*]

[1]*Institute of Materials, Biology and Environment, Academy of Military Science and Technology, 17 Hoang Sam Street, Nghia Do Ward, Hanoi, Vietnam*
[2]*Institute of Materials Science, Vietnam Academy of Science and Technology, 18 Hoang Quoc Viet Street, Nghia Do Ward, Hanoi, Vietnam*
[3]*Department of Military Science, Ministry of National Defence of Vietnam, 28A Dien Bien Phu Street, Ba Dinh Ward, Hanoi, Vietnam*

Received 21 August 2025; revised 1 September 2025; accepted 25 October 2025

Abstract:

In this study, ZnO nanomaterials were synthesised via a hydrothermal method and characterised using X-ray diffraction (XRD), scanning electron microscopy (SEM)/high-resolution transmission electron microscopy (HRTEM), Brunauer-Emmett-Teller (BET), analysis and diffuse reflectance spectroscopy (DRS). The obtained ZnO exhibited a wurtzite structure, high crystallinity, mesoporosity, a large specific surface area of 107.17 m^2/g, and a band gap of 3.19 eV. Photocatalytic performance was comparatively evaluated under visible and UV irradiation using methylene blue (MB) and Rhodamine B (RhB) as model dyes. ZnO achieved >90-98% degradation, with consistently faster kinetics under UV irradiation and MB degrading faster than RhB. Pseudo-first-order fits yielded k(MB)=0.027 min^{-1} (Vis) vs 0.076 min^{-1} (UV) and k(RhB)=0.024 min^{-1} (Vis) vs 0.066 min^{-1} (UV), linking structure-property features to light-dependent activity. These results establish a clear UV/Vis comparison and underscore the applicability of hydrothermal ZnO for wastewater treatment under practical illumination.

Keywords: **methlyene blue, organic dye degradation, photocatalysis, rhodamine B, visible light, ZnO nanomaterials.**

Classification numbers: **2.2, 2.3, 5.3**

1. Introduction

Organic dyes released from the textile, paper, plastic, and food industries have become a major source of environmental pollution and represent a pressing global concern. These dyes are often toxic, persistent, and pose serious risks to aquatic ecosystems and human health. Therefore, the development of efficient methods for the removal or degradation of such organic pollutants is of critical importance [1, 2]. Among the various treatment techniques available, photocatalytic degradation has emerged as one of the most effective approaches for eliminating organic dyes from wastewater [3, 4].

In recent years, nanotechnology has opened new avenues for environmental remediation, particularly through the use of semiconductor metal oxides such as TiO_2, ZnO, CuO, Fe_3O_4, Cr_2O_3, Co_3O_4, and MnO_2 as photocatalysts [5, 6]. ZnO is an n-type semiconductor with a relatively wide band gap (~3.2 eV) and a high exciton binding energy (~60 meV) at room temperature [7]. It possesses several advantageous properties, including high chemical stability, non-toxicity, low cost, and strong light absorption across a broad spectrum [8-10]. In particular, ZnO nanomaterials with reduced crystallite size and large specific surface area provide more active sites compared to their bulk counterparts, demonstrating superior potential for photocatalytic applications [11, 12].

The photocatalytic performance of ZnO is strongly influenced by its particle size and morphology [13]. Therefore, controlling the shape and size of ZnO nanoparticles is essential. Various synthesis methods have been explored for ZnO fabrication, including hydrothermal synthesis, sol-gel methods, and precipitation techniques. Among them, the hydrothermal method offers significant advantages such as low-temperature operation and the production of highly pure ZnO. This method also allows for effective morphology tuning by adjusting synthesis parameters such as reaction temperature, duration, solvent type, and precursor characteristics. As a result, a wide range of ZnO morphologies - such as flower-like, rod-like, and spherical structures-can be obtained [13-15].

This study reports the synthesis and optimisation of ZnO nanomaterials, with particular emphasis on a comparative evaluation of methylene blue degradation under UV and visible light. The findings highlight the potential of ZnO for visible-light-driven photocatalysis in sustainable wastewater treatment.

2. Materials and methods

2.1. Materials

Zinc sulphate heptahydrate ($ZnSO_4 \cdot 7H_2O$, 99%), urea ($(NH_2)_2CO$, 98%), and ethanol (C_2H_5OH, 99%) were purchased from Xilong Chemicals (China) and used without further purification. Deionised water was used as the solvent.

*Corresponding author: Email: chinhpkkq@gmail.com

2.2. Synthesis of ZnO nanomaterials

Porous ZnO nanomaterials were synthesised via a hydrothermal method under modified reaction and calcination conditions. Briefly, 10 mmol of zinc sulphate heptahydrate ($ZnSO_4 \cdot 7H_2O$) was dissolved in 30 ml of deionised water under magnetic stirring for 15 min. Then, 20 ml of an aqueous solution containing 20 mmol of urea was added dropwise, and the mixture was stirred for another 15 min to adjust the pH to ~5. The homogeneous solution was transferred to a 100 ml Teflon-lined stainless-steel autoclave and heated at 220°C for 24 h. After natural cooling to room temperature, the resulting white precipitate was collected by centrifugation, washed repeatedly with deionised water and twice with ethanol, and dried at 60°C for 24 h. Finally, the dried ZnO precursor was annealed at 400°C for 2 h in air to improve crystallinity.

2.3. Characterisation of the material properties

The morphology of the ZnO nanomaterials was examined using SEM (Hitachi S-4800), while microstructural features and lattice fringes were analysed by HRTEM (JEM-2100, JEOL). Crystal structure was determined by XRD (Bruker D8 Advance) using Cu-Kα radiation (λ=1.54 Å) at 40 kV and 44 mA over a 2θ range of 10°-80°. Specific surface area and pore characteristics were measured by the BET method (Quantachrome NOVA Touch 2LX). Optical absorption properties were evaluated by UV-Vis diffuse reflectance spectroscopy (DRS) in the 200-800 nm range.

2.4. Photocatalytic activity investigation

The photocatalytic activity of the ZnO nanomaterials was evaluated through the degradation of MB and RhB under simulated sunlight (compact fluorescent lamp, 105 W) and UV irradiation (UVP XX-40BLB, 365 nm). In each experiment, 0.03 g of ZnO was dispersed in 50 ml of 10 mg/l MB or RhB solution in a transparent glass tube. Prior to illumination, the suspension was kept in the dark for 1 hour to establish adsorption-desorption equilibrium. The samples were then irradiated under air circulation, and aliquots were collected at predetermined time intervals. The suspensions were filtered to remove the catalyst, and the residual dye concentrations were measured using UV-Vis spectrophotometry (Drawell DV-8200) at 664 nm for MB and 554 nm for RhB.

The degradation efficiency (%) of MB and RhB at time t was calculated using the equation [9]:

$$H(\%) = \frac{C_o - C_t}{C_o}.100\%$$

where C_0 and C_t represent the initial and time-dependent dye concentrations, respectively.

3. Results and discussion

3.1. Characterisation of ZnO nanomaterials

The XRD pattern of the ZnO material synthesised via the hydrothermal method is shown in Fig. 1A. Distinct and sharp diffraction peaks are observed at 2 θ values of approximately 31.7°, 34.4°, 36.2°, 47.5°, 56.6°, 62.9°, 66.4°, 68.0°, 72.6°, 77.0°, and 81.5°. These peaks correspond to the (100), (002), (101), (102), (110), (103), (200), (112), (201), and (202) crystal planes, respectively. The lattice parameters of ZnO were calculated from the (100), (002), and (101) diffraction peaks using Bragg's law and the hexagonal relation. The obtained values were a=b=3.251 Å and c=5.207 Å, which are consistent with the standard wurtzite phase (JCPDS No. 36-1451: a=b=3.26 Å, c=5.21 Å [10]). The average crystallite size of ZnO was estimated using the Debye-Scherrer equation $D=K\lambda/(\beta\cos\theta)$, where K=0.9, λ=0.15406 nm (Cu Kα radiation), θ is the Bragg angle, and β is the corrected FWHM in radians. The instrumental broadening (βi=0.10°) was subtracted from the observed FWHM (βobs) using $\beta=(\beta obs^2-\beta i^2)1/2$ [16]. The corrected β values were converted into radians (β=0.0070 rad for the (101) peak at 2 θ=36.2°) and the calculated crystallite size was approximately 20.9 nm, confirming the nanocrystalline nature of the synthesised ZnO.

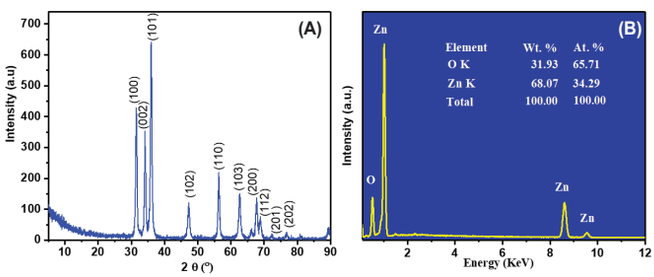

Fig. 1. (A) XRD pattern and (B) EDX spectrum of the ZnO nanomaterials used in this study.

The elemental composition determined from the EDX spectrum is presented in Fig. 1B. In this spectrum, only the characteristic peaks of Zn and O are observed. The deviation from the ideal 1:1 Zn/O atomic ratio is attributed to the surface-sensitive nature of EDX, where excess oxygen may arise from surface hydroxyl groups and adsorbed water. The absence of any additional elemental peaks confirms the high purity of the ZnO sample, which is consistent with the XRD results.

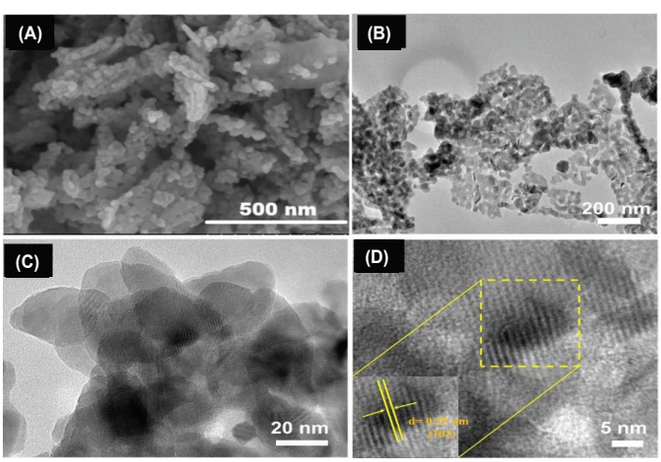

Fig. 2. (A) SEM image, and (B, C, D) HR TEM images of the ZnO nanomaterials used in this study.

As shown in the SEM image (Fig. 2A), the ZnO sample exhibits a porous architecture consisting of densely packed and relatively uniform particle clusters. The constituent particles display predominantly spherical to short rod-like morphologies, with diameters in the range of approximately 20-30 nm. The rough surface texture and interconnected network with abundant voids are expected to enhance surface-dependent processes, making the material suitable for applications in adsorption, sensing, and catalysis. High-resolution transmission electron microscopy (HRTEM) reveals well-defined lattice fringes with an interplanar spacing of 0.25 nm, corresponding to the (101) plane of the wurtzite ZnO structure. The absence of observable structural defects or amorphous shells around the particles further confirms the high crystallinity and structural uniformity of the synthesised ZnO.

The N_2 adsorption-desorption isotherm and pore size distribution of ZnO are presented in Fig. 3A. The isotherm exhibits a type IV profile according to the IUPAC classification, which is characteristic of mesoporous materials. The pore size distribution, calculated using the BJH method, indicates that the majority of the pores fall within the range of 2-5 nm, with a prominent peak centred at approximately 1.83 nm, confirming that the material lies within the lower mesoporous range. The narrow pore size distribution, together with a total pore volume of 0.3354 cm^3/g, suggests a well-developed and uniform mesoporous network. The specific surface area of the material, determined by the BET method, is 107.17 m^2/g. This relatively high surface area is beneficial for enhancing adsorption capacity and increasing the number of accessible active sites. These structural and textural features render the material highly suitable for a variety of applications, including photocatalysis, gas sensing, environmental adsorption, and as electrode materials in batteries and supercapacitors.

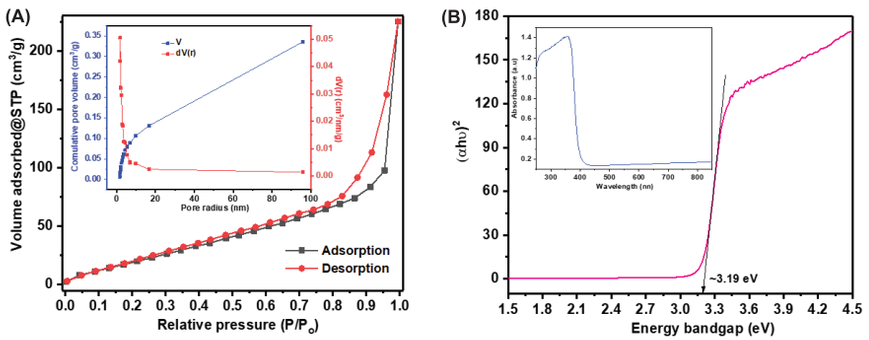

Fig. 3. (A) N_2 adsorption-desorption isotherm and pore size distribution (inset); (B) Tauc plot and UV-Vis DRS spectrum (inset) of ZnO nanomaterials.

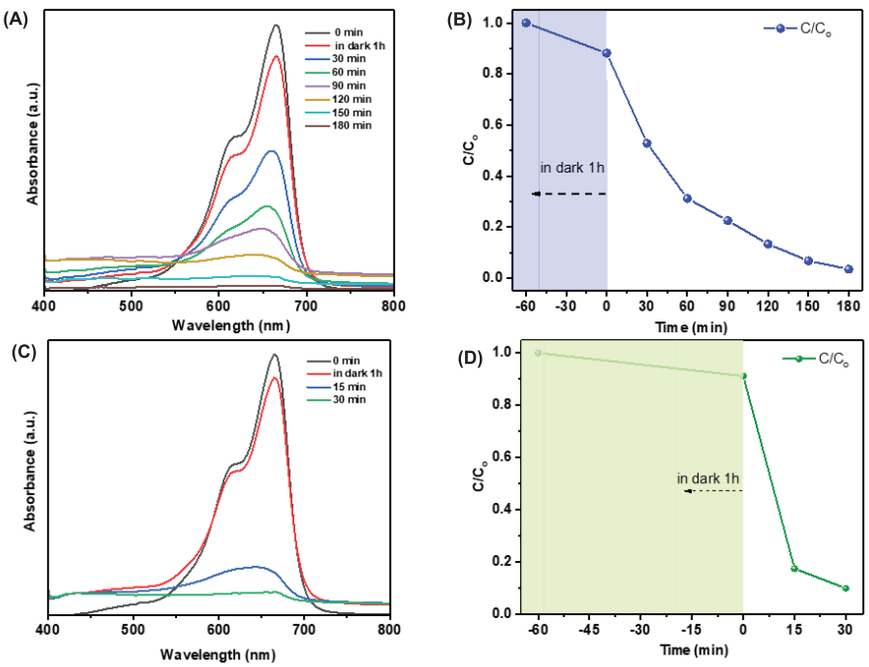

Fig. 4. UV-Vis absorption spectra and photocatalytic degradation of methylene blue using ZnO nanomaterials under visible (A, B) and UV (C, D) light irradiation.

The optical band gap energy of the synthesised ZnO material was estimated using UV-Vis diffuse reflectance spectroscopy (DRS), as illustrated in Fig. 3B. The inset shows the absorbance spectrum, which reveals a sharp absorption edge in the UV region around 380 nm, indicative of strong UV-light absorption. To determine the optical band gap (E_g), the Tauc plot method was employed by plotting $(\alpha h\nu)^2$ versus photon energy ($h\nu$), assuming a direct allowed transition for ZnO. The linear region of the plot was extrapolated to the photon energy axis, where $(\alpha h\nu)^2=0$, yielding an estimated bandgap energy of approximately 3.19 eV. This value is consistent with the reported bandgap of wurtzite ZnO, typically ranging 3.1-3.3 eV [9], and confirms the material's semiconducting nature with efficient UV-light absorption characteristics.

3.2. Evaluation of photocatalytic activity

The photocatalytic performance of the ZnO nanomaterials was evaluated through the degradation of methylene blue (MB) under both visible and UV light irradiation. The results are presented in Fig. 4.

Under visible light (Figs. 4A and B), the characteristic absorption peak of MB at ~664 nm gradually decreased with irradiation time. After 180 minutes, the absorbance nearly vanished, indicating

efficient photodegradation. The corresponding C/C_0 value decreased from ~0.95 to ~0.08, yielding a degradation efficiency of approximately 92%. Notably, during the 1-hour dark adsorption period, the MB concentration remained nearly unchanged, confirming negligible adsorption and that the degradation primarily occurred under illumination.

In contrast, under UV light (Figs. 4C and D), the degradation occurred much more rapidly. The MB absorbance significantly diminished after just 30 minutes, with C/C_0 decreasing from ~0.95 to ~0.05, corresponding to a 95% degradation efficiency. Again, no significant change was observed during the dark phase, reinforcing that the process was photocatalytic rather than adsorptive.

These findings confirm that ZnO exhibits photocatalytic activity under both visible and UV light, with markedly higher efficiency under UV illumination. This enhancement can be attributed to the wide band gap of ZnO (~3.2 eV), which allows more efficient generation of electron-hole pairs and subsequent formation of reactive oxygen species under UV light, thereby accelerating the degradation process.

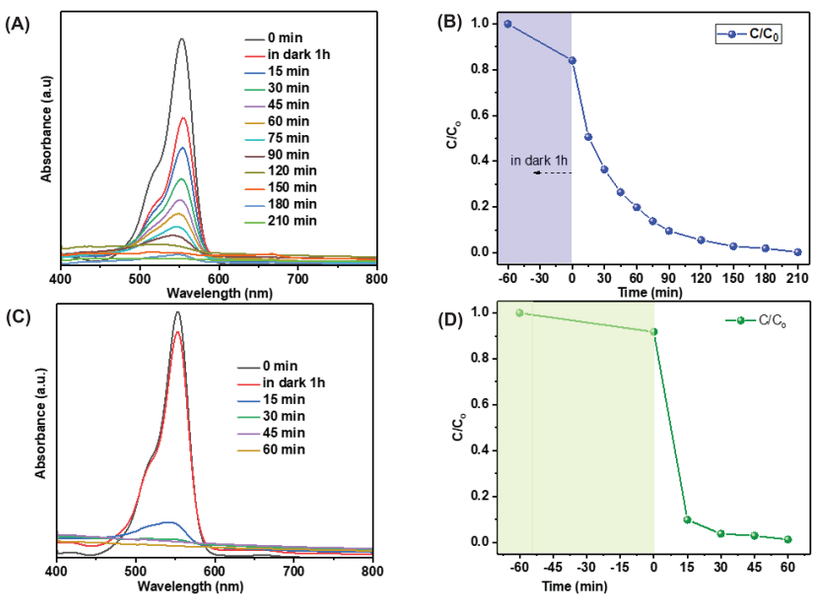

Fig. 5. UV-Vis absorption spectra and photocatalytic degradation of Rhodamine B using ZnO nanomaterials under visible (A, B) and UV (C, D) light irradiation.

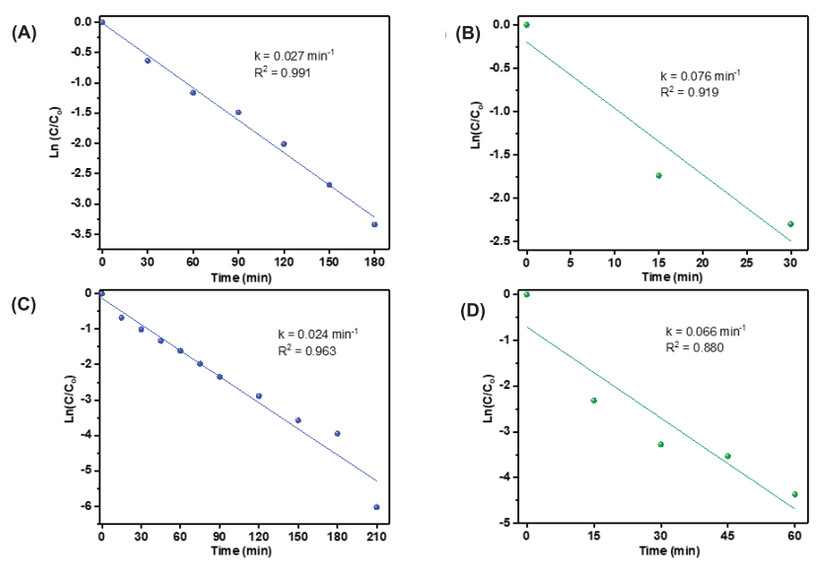

Fig. 6. Kinetic study of degradation of MB under (A) visible, (B) UV light, and RhB under (C) visible, (D) UV light irradiation.

Following the successful degradation of methylene blue (MB) discussed in Fig. 4, the photocatalytic performance of ZnO nanomaterials was further evaluated using Rhodamine B (RhB) as a second model pollutant under identical experimental conditions. The corresponding UV-Vis spectra and degradation profiles are presented in Fig. 5.

Under visible light irradiation (Figs. 5A and 5B), the absorption peak of RhB cantered at ~554 nm decreased gradually with time. Complete degradation was achieved after approximately 210 minutes, as the C/C_0 value dropped from ~1.0 to ~0.03, corresponding to a 97% degradation efficiency. However, this required a longer irradiation time compared to MB, which reached ~92% degradation within 180 minutes (Fig. 4B), suggesting that MB degraded more rapidly under the same visible-light conditions.

Under UV irradiation (Figs. 5C and D), RhB degradation occurred more efficiently than under visible light, but still at a slower rate than MB. After 60 minutes of UV exposure, the C/C_0 value of RhB decreased from ~0.95 to ~0.02, corresponding to a 98% degradation efficiency. In contrast, MB achieved 95% degradation within just 30 minutes under UV light (Fig. 4D). This indicates that, although both dyes were effectively degraded, MB exhibited faster kinetics than RhB under identical UV conditions.

Importantly, in both visible and UV light experiments, the 1-hour dark adsorption phase showed a negligible decrease in dye concentration for both MB and RhB, confirming that photocatalytic degradation, rather than physical adsorption, was the dominant removal mechanism.

The photocatalytic kinetics were evaluated using a pseudo-first-order model, $\ln(C/C_0)=-kt$, where C_0 and C are the dye concentrations at the initial time and at time t (min), respectively, and k is the apparent rate constant (min^{-1}).

The kinetic analysis (Fig. 6) shows that the degradation of MB and RhB follows a pseudo-first-order model with high correlation coefficients (R^2=0.880-0.991). The reaction rate of MB under visible light (k=0.027 min^{-1}) is lower than that under UV irradiation (k=0.076 min^{-1}). Similarly, RhB exhibits a slower degradation rate under visible light (k=0.024 min^{-1}) compared with UV light (k=0.066 min^{-1}). These results confirm that ZnO displays higher photocatalytic efficiency in the UV region, which is consistent with its band gap energy (~3.2 eV) favouring strong UV absorption. Nevertheless, the observable activity under visible light also highlights the potential applicability of the material under natural illumination.

The observed difference in degradation rates between MB and RhB can be attributed to their molecular structures. RhB possesses a bulkier xanthene-based framework with greater photostability and steric hindrance, rendering it more resistant to oxidative degradation by reactive oxygen species (ROS) such as •OH and $•O_2^-$. In contrast, MB has a simpler phenothiazine structure, making it more susceptible to ROS-induced breakdown.

4. Conclusions

In this study, ZnO nanomaterials were successfully synthesised via a hydrothermal method and comprehensively characterised. The obtained material exhibited a hexagonal wurtzite structure, high crystallinity, nanoscale morphology, and a high specific surface area with a well-developed mesoporous network. These physicochemical properties contributed to the material's excellent photocatalytic activity. Photocatalytic experiments demonstrated that ZnO was highly effective in degrading both MB and RhB under visible and UV light irradiation. Under identical conditions, MB consistently showed faster degradation rates than RhB, highlighting the influence of dye molecular structure on photocatalytic kinetics. Overall, the results confirm that the synthesised ZnO nanomaterials possess strong potential for environmental remediation, particularly in the photodegradation of organic pollutants from wastewater using solar- or visible-light-based systems.

CRediT author statement

Nguyen Thi Phuong: Investigation, Data analysis, Methodology, Writing and Reviewing; Lai Van Duy: Validation, Formal analysis, Writing, Reviewing and Editing; Tran Van Chinh: Methodology, Conceptualisation, Supervision, Writing original draft.

COMPETING INTERESTS

The authors declare that there is no conflict of interest regarding the publication of this article.

REFERENCES

[1] A. Houas, H. Lachheb, M. Ksibi, et al. (2001), "Photocatalytic degradation pathway of methylene blue in water", *Applied Catalysis B: Environmental*, **31(2)**, pp.145-157, DOI: 10.1016/S0926-3373(00)00276-9.

[2] C. Hou, B. Hu, J. Zhu (2018), "Photocatalytic degradation of methylene blue over TiO_2 pretreated with varying concentrations of NaOH", *Catalysts*, **8(12)**, DOI: 10.3390/catal8120575.

[3] R. Ghamarpoor, A. Fallah, M. Jamshidi (2024), "A review of synthesis methods, modifications, and mechanisms of ZnO/TiO_2-based photocatalysts for photodegradation of contaminants", *ACS Omega*, **9(24)**, pp.25457-25492, DOI: 10.1021/acsomega.3c08717.

[4] M. Dolatyari, M. Tahmasebi, S. Dolatyari, et al. (2024), "Core/Shell ZnO/TiO_2, SiO_2/TiO_2, Al_2O_3/TiO_2, and $Al_{1.9}Co_{0.1}O_3$/TiO_2 Nanoparticles for the photodecomposition of brilliant blue E-4BA", *Inorganics*, **12(11)**, DOI: 10.3390/inorganics12110281.

[5] Y. Zhou, Z. Wang, X. Li, et al. (2025), "Synthesis of leek-based N, S self-doped CQDs/TiO_2 and its application in the photocatalytic degradation of organic pollutants", *Materials Science in Semiconductor Processing*, **185**, DOI: 10.1016/j.mssp.2024.108864.

[6] F. Gomaa, M. Mohammed (2025), "Eco-friendly synthesis of CuO/PMMA nanocomposite films for efficient Rhodamine B dye photocatalytic degradation", *Journal of Inorganic Organometallic Polymers Materials*, pp.1-23, DOI: 10.1007/s10904-025-03613-x.

[7] Z. Yang, Z. Ye, B. Zhao, et al. (2010), "Synthesis of ZnO nanobundles via sol-gel route and application to glucose biosensor", *Journal of Sol-Gel Science Technology*, **54(3)**, pp.282-285, DOI: 10.1007/s10971-010-2191-z.

[8] A. Akyol, H. Yatmaz, M. Bayramoglu (2004), "Photocatalytic decolorization of Remazol Red RR in aqueous ZnO suspensions", *Applied Catalysis B: Environmental*, **54(1)**, pp.19-24, DOI: 10.1016/j.apcatb.2004.05.021.

[9] N.H. Hanh, Q.T.M. Nguyet, T.V. Chinh, et al. (2024), "Enhanced photocatalytic efficiency of porous ZnO coral-like nanoplates for organic dye degradation", *RSC Advances*, **14(21)**, pp.14672-14679, DOI: 10.1039/D4RA01345J.

[10] D.D. La, D.V. Lai, N.T.M. Quan, et al. (2025), "Enhanced photocatalytic performance of ZnO nanoparticles functionalized with 5-(4′-carboxyphenyl)-10, 15, 20-triphenylporphyrin-zinc", *Materials Research Bulletin*, **185**, DOI: 10.1016/j.materresbull.2025.113326.

[11] S. Cherif, H.R. Yazid, S. Hemidouche, et al. (2025), "Comparative study on the photocatalytic efficiency of ZnO nanoparticles synthesized via chemical and eco-friendly coprecipitation methods", *Ceramics International*, **51(4)**, pp.4737-4749, DOI: 10.1016/j.ceramint.2024.11.448.

[12] A.N. Tuama, L.H. Alzubaidi, M.H. Jameel, et al. (2024), "Impact of electron-hole recombination mechanism on the photocatalytic performance of ZnO in water treatment: A review", *Journal of Sol-Gel Science Technology*, **110(3)**, pp.792-806, DOI: 10.1007/s10971-024-06385-x.

[13] A.K. Radzimska, T. Jesionowski (2014), "Zinc oxide - from synthesis to application: A review", *Materials*, **7(4)**, pp.2833-2881, DOI: 10.3390/ma7042833.

[14] J. Blancas, N.C. Castro, R. Pérez, et al. (2024), "A novel hydrothermal approach to preparing ZnO flower-like using CQDs as growth seeds", *Materials Science and Engineering: B*, **309**, DOI: 10.1016/j.mseb.2024.117654.

[15] T. Wang, L. He, J. Zhang, et al. (2025), "Effects of ZnO morphology on tribological behaviors of polyarylene ether nitrile composites", *Composite Structures*, **354**, DOI: 10.1016/j.compstruct.2024.118810.

[16] D.M. Herrera, M. Pal (2022), "A comprehensive study of X-ray peak broadening and optical spectrum of Cu_2ZnSnS_4 nanocrystals for the determination of microstructural and optical parameters", *Applied Physics A*, **128(11)**, DOI: 10.1007/s00339-022-06137-0.